



Effect of sulfidation temperature on the intrinsic activity of Co–MoS₂ and Co–WS₂ hydrodesulfurization catalysts

Yasuaki Okamoto^{a,*}, Akira Kato^a, Usman^{a,1}, Nino Rinaldi^a, Takashi Fujikawa^b, Hiromichi Koshika^c, Ichiro Hiromitsu^a, Takeshi Kubota^a

^a Department of Material Science, Shimane University, Matsue 690-8504, Japan

^b Research and Development Center, Cosmo Oil Co. Ltd., Satte 340-0193, Japan

^c Central Research Laboratories, Idemitsu Kosan Co. Ltd., Sodegaura 299-0293, Japan

ARTICLE INFO

Article history:

Received 7 January 2009

Revised 27 April 2009

Accepted 4 May 2009

Available online 4 June 2009

Keywords:

Hydrodesulfurization

Co–Mo sulfide catalyst

Co–W sulfide catalyst

Active site structure

Turnover frequency

Magnetic property

Sulfidation temperature

Temperature-programmed sulfidation

XAFS

ABSTRACT

The effect of presulfidation temperature on the magnetic property, local structure, and intrinsic hydrodesulfurization activity of Co–Mo(W)–S has been studied with SiO₂-supported Co–Mo and Co–W sulfide catalysts prepared by exposing presulfided MoS₂/SiO₂ and WS₂/SiO₂, respectively, to a vapor of Co(CO)₃NO. A TPS study shows that complete sulfidation of Mo(W) precursors to Mo(W)S₂ particles is required for the formation of Co–Mo(W)–S Type II. The intrinsic activity of Co–W–S Type II is 1.6 times as high as that of Co–Mo–S Type II. The Co K-edge EXAFS analysis of Co–Mo(W)–S confirms the formation of dinuclear Co sulfide clusters on Mo(W)S₂ edges. The intrinsic activity of Co–Mo–S is correlated with the Co–S–Co antiferromagnetic interaction strength, suggesting modifications of the electronic state and local structure of Co–Mo–S by MoS₂–O-support interactions, in conformity with the EXAFS analysis.

© 2009 Elsevier Inc. All rights reserved.

1. Introduction

Hydrodesulfurization (HDS) catalysts have been playing vital roles in protecting the environment by reducing sulfur in fuel oils to as low as 10 ppm, and thereby enabling the development of novel catalyst systems for the abatements of NO_x and particulate matter in the effluent gases from combustion engines, in particular, diesel engines. Improving the performance of HDS catalysts is still one of the most urgent issues in petroleum industry [1,2]. Supported Mo sulfides promoted by Co or Ni and W sulfides promoted by Ni have been widely used in industry for HDS reaction [2–4]. The knowledge on the number of the active sites and their intrinsic activity is of inevitable importance from the point of catalysis science and for the sake of rational design and development of HDS catalysts with improved performance. In the case of Co(Ni)–Mo(W) sulfide catalysts, it is generally accepted that the so-called Co–Mo–S phase (structure), in which Co atoms are located on the edge of MoS₂ particles, is the active site [5,6]. The formation of

Co–Mo–S accounts for the generation of strong catalytic synergies between Co(Ni) and Mo sulfides. The precise local structure of Co–Mo–S is, however, still under debate [3,7].

Practical Co–Mo HDS catalysts are generally composed of several phases: Co₉S₈ nanoparticles, Co²⁺ species strongly interacting with the support, Mo (oxy)sulfides as well as Co–Mo–S [3–6]. Without using sophisticated techniques such as MES (Mössbauer emission spectroscopy), however, it is not easy to obtain the information on the intrinsic activity of the active sites of HDS catalysts [3,4]. In addition, Co–Mo–S is at least classified into two types depending on the intrinsic activity: Type I and Type II, the latter showing activity that is about twice higher than that shown by the former. On the basis of the number of Co–Mo–S obtained using MES, it was shown with alumina-supported catalysts that Co–Mo–S Type II is formed by sulfidation above 875 K, while Type I is prepared at 675 K [5,6,8]. Several groups suggested that full sulfidation of Mo oxides to MoS₂ is a prerequisite for the formation of Co–Mo–S Type II [6,8–10].

It has been shown in the above context that the intrinsic activity of Co–Mo–S depends on the metal sulfide-support interactions [3,4]. Van Veen et al. [11] using MES found that the addition of phosphorus to Co–Mo/Al₂O₃ increases the intrinsic activity of Co–Mo–S by about 1.5 times, suggesting that a part of Co–Mo–S Type I is changed to Type II. In line with their MES study, Usman

* Corresponding author. Fax: +81 852 32 6466.

E-mail address: yokamoto@riko.shimane-u.ac.jp (Y. Okamoto).

¹ Present address: Haluoleo University, Jurusan Kimia, FMIPA, Kampus Bumi Tridharma, Anduonohu, Kendari, Indonesia.

et al. [12] showed a similar increase in the intrinsic activity of Co–Mo–S for the HDS of thiophene by the addition of phosphorus using the Co(CO)₃NO–CVD technique. Similarly, Usman et al. [13] found a 1.6 times increase of the intrinsic activity by the addition of boron. It was shown with Co–Mo/B₂O₃–Al₂O₃ [14] that the intrinsic activity of Co–Mo–S is proportional to that of MoS₂, which was evaluated by NO adsorption capacity, and that the intrinsic activity of Co–Mo–S increases as the basic hydroxyl groups on Al₂O₃ are consumed by the addition of boron. van Veen et al. [15] and Usman et al. [12] suggested a similar trend for phosphorus-added catalysts. In this sense, it is considered that the intrinsic activity of Co–Mo–S is a function of the number of strong MoS₂–O–Al linkages in MoS₂ particles or the density of the linkages, as suggested by Hensen et al. [16]. DFT calculations on MoS₂ by Hinneemann et al. [17] suggested that the energy to remove sulfur atoms to form coordinatively unsaturated Mo sites is increased by the MoS₂–O–Al linkages, thus reducing the intrinsic activity of MoS₂. Arrouvel et al. [18] and Costa et al. [19] have shown by extensive DFT studies that the interaction modes of MoS₂ clusters with Al₂O₃ or TiO₂ surface as well as their composition depend on the chemical potential of sulfur (P_{H₂S}/P_{H₂} and T) and cluster size. They suggested that for γ -Al₂O₃ most MoS₂ particles with an edge length larger than 1 nm lie in a parallel configuration on the support and the chemical ligand effect of the support vanishes [18]. Costa et al. [19] suggested that Co weakens the edge anchoring of the active phase.

The formation of Co–Mo–S Type I and Type II was claimed on the basis of the HDS activity and the number of Co–Mo–S as evaluated by MES for Co–Mo catalysts [8–10]. However, Type I and Type II have very close Mössbauer parameters and therefore cannot be discriminated by MES techniques alone [11,20,21]. The XPS binding energy of Co2p levels is also insensitive to the type and support as revealed by Bouwens et al. [10]. In agreement with this, essentially the same Co2p binding energies were observed for Co–Mo–S supported on Al₂O₃ and SiO₂ in spite of a considerable difference in the intrinsic activity [22]. The EXAFS analysis by Bouwens et al. [10] presented some possibility to discriminate Co–Mo–S Type I and Type II with the Co–S coordination number for Type II being larger than that for Type I. They suggested a positive correlation between the Co–S coordination number and the specific thiophene HDS activity (activity per mol Co). It seems that the physicochemical characterization of Co–Mo–S Type I and Type II is not enough to differentiate and specify them at present. In the present study, we propose that the magnetic property of Co–Mo–S provides an important clue to specify their nature.

Supported W sulfide catalysts promoted by Ni have also been extensively studied because of the generation of strong catalytic synergies between W and Ni [2–4]. On the other hand, Co–W sulfide catalysts have received much less attention than the other three combinations due to much weaker promotional effects of Co in conventionally prepared Co–W catalysts [23–27]. One of the reasons for the weak promotional effects of Co is suggested to be due to a lower coverage of Co on the edge of WS₂ particles since the sulfidation temperature of Co oxides is much lower than that of W oxides [24,26]. The use of a chelating agent, which forms a complex with Co, improved the HDS activity of Co–WS₂ catalysts, possibly, by increasing the number of Co atoms on the edge of WS₂ particles because of the decrease in the difference between the sulfidation temperatures of Co and W [24–26]. The increase of the fraction of Co on the WS₂ edge was evidenced by Co K-edge XANES spectra when NTA (nitritoltriacetic acid) was added as a chelating agent [26]. The active sites of Co–WS₂ catalysts, Co–W–S, are much less characterized in comparison with Co–Mo–S. In our previous study [27], we compared the intrinsic activities of Co–Mo–S and Co–W–S for the HDS of thiophene as a function of the presulf-

idation temperature of Mo(W)S₂/SiO₂ (673–873 K). When the presulfidation temperature was below 773 K, the intrinsic activity of Co–W–S was lower than that of Co–Mo–S. However, when the presulfidation temperature was raised to 873 K, the intrinsic activity of Co–W–S was almost the same as or even slightly higher than that of Co–Mo–S. Nevertheless, to obtain deeper insights into the nature of the active phase, a more extensive study is needed on the effect of presulfidation temperature on the intrinsic activity of Co–Mo–S and Co–W–S.

In the present study, we extend our previous study [27] and extensively explore the effect of the presulfidation temperature (673–1173 K) of MoS₂ and WS₂ particles on the intrinsic activity of SiO₂-supported Co–Mo–S and Co–W–S, respectively, to obtain deeper insights into the origin and physicochemical properties of Type I and Type II. The Co–Mo catalysts are characterized by magnetic measurements, TEM, XAFS, and TPS. We stress in the current study that the intrinsic activity, electronic state, and local structure of Co–Mo–S are determined by the MoS₂–O–support interactions. Besides, it is demonstrated that a Co–WS₂ combination is more favorable than a conventional Mo counterpart. It is found that the intrinsic activity of Co–Mo–S for thiophene HDS is correlated with the magnetic property of Co–Mo–S.

2. Experimental

2.1. Catalyst preparation

In the present study, we admitted Co to the supported MoS₂ catalysts using the CVD technique [22,27] to prepare Co–Mo sulfide catalysts instead of using a conventional impregnation technique. 10 wt% MoO₃/SiO₂ (6.7 wt% Mo) and 20 wt% WO₃/SiO₂ (15.9 wt% W) (SiO₂, 370 m²/g) were prepared in an analogous way to the previous study by an impregnation method using (NH₄)₆Mo₇O₂₄·4H₂O and (NH₄)₆W₁₂O₃₉·5H₂O as precursors, respectively [27]. The MoO₃/SiO₂ or WO₃/SiO₂ catalyst thus prepared was presulfided at 673–1173 K in a 10% H₂S/H₂ flow at an atmospheric pressure for 2 h. The Mo(W) sulfide catalyst is designated as Mo(W)/Si followed by the presulfidation temperature in parentheses, when necessary. Cobalt was introduced to Mo/Si and W/Si by using the CVD technique [22,27]. Briefly, Mo/Si was first evacuated at 673 K for 1 h and was subsequently exposed for 5 min at room temperature to a vapor of Co(CO)₃NO kept at 273 K. After evacuation at room temperature, the sample was sulfided again at 673 K for 1.5 h to prepare Co/Mo/Si regardless of the presulfidation temperature of Mo/Si. Co/W/Si was also prepared in the same manner. The amount of Co incorporated by the CVD technique was determined within an accuracy of $\pm 5\%$ by means of XRF (Shimadzu EDX-700HS).

Another Mo/Si (6.7 wt% Mo) was also prepared by the impregnation of SiO₂ with (NH₄)₂MoS₄ (ATM, Kanto Chemicals) dissolved in *N,N*-dimethylformamide. After a one-night impregnation, the solvent was removed by evaporation at room temperature under gentle stirring (several days) to suppress the oxidation of the thiomolybdate. The dried material was treated in a 10% H₂S/H₂ stream at 673 K for 2 h. Mo/Si thus prepared is designated as Mo/Si (ATM) hereafter. Co/Mo/Si (ATM) was prepared by the CVD method as described above.

For magnetic measurements, Al₂O₃- and B₂O₃–Al₂O₃-supported Co/Mo catalysts (13 wt% MoO₃) were prepared by the CVD method according to the previous study [13]. They are denoted as Co/Mo/Al and Co/Mo/B–Al, respectively.

2.2. Reaction procedure

The initial activity of the freshly prepared catalyst for the HDS of thiophene was evaluated at 623 K using a circulation reaction

system made of glass under mild reaction conditions (initial H₂ pressure, 20 kPa) [22,27]. The reaction products were mainly H₂S, butenes, and *n*-butane. The HDS activity was calculated on the basis of the accumulated amount of H₂S. The detailed reaction procedures have been reported previously [22]. The catalytic activity was reproducible within an accuracy of $\pm 5\%$.

2.3. Characterization

2.3.1. Temperature-programmed sulfidation (TPS)

The TPS apparatus used in the present study has been described previously [28]. The composition of the sulfiding gas was 2.7% H₂S, 30.3% H₂, and 67.0% Ar (H₂S/H₂ = 0.089). The total pressure of the gas in the TPS reactor was regulated at 0.118 MPa. The H₂S concentration in the reactant gas was analyzed with a UV spectrophotometer (Japan Spectroscopic, 875-UV). The H₂ concentration was determined by a thermal conductivity detector (Okura Riken, 802T) after H₂S and H₂O had been removed by a 5A molecular sieve trap. The oxide sample (10 wt% MoO₃/SiO₂ and 20 wt% WO₃/SiO₂) in a quartz tube reactor was purged with a pure Ar flow for more than 60 min. Then the Ar flow was replaced by the sulfiding gas at 300 K for 90 min. Subsequently, the temperature was increased up to 1300 K at a constant heating rate (5 K/min), followed by an isothermal sulfidation at 1300 K for 60 min.

2.3.2. Transmission electron microscopy (TEM)

TEM images of Mo/Si were taken on an electron microscope JEM-2010 with an accelerating voltage of 200 keV. The Mo/Si powder sample was evacuated and sealed in a glass tube without exposure to air. The catalyst sample was suspended in acetone and placed on a specimen grid in a glove-bag filled with N₂ to avoid contact with air. The sample was then transferred in a stream of N₂ to a sample holder attached to the microscope. The distributions of MoS₂ particle size and stacking number were calculated over 200–250 particles in several arbitrary chosen areas.

2.3.3. Magnetic measurements

The static magnetic susceptibility measurements of sulfided Co/Mo catalysts were done in situ with a Faraday method using a Cahn 2000 Electro-Balance system between 4.2 K and 300 K [29]. The catalyst sample was evacuated at 673 K for 1 h before fusing into a quartz glass ampoule. The magnitude of the magnetic field was fixed at 10000 G. The effective magnetic moment and magnetic susceptibility of Co were obtained by subtracting the magnetic contributions of the quartz glass ampoule and the corresponding MoS₂ sample separately measured under the identical conditions.

2.3.4. X-ray absorption fine structure (XAFS)

The Co K-edge XAFS spectra of the catalysts and reference compounds were measured at room temperature at BL-7C and BL-9C of KEK-IMSS-PF (Institute of Material Structure Science, High Energy Accelerator Research Organization, Photon Factory) using an in situ XAFS cell in a fluorescence mode with 2.5 GeV ring energy and 250–290 mA stored current by using a Litle-type detector [26]. The EXAFS data were analyzed using a program REX2000 (Rigaku Co.). The analysis involves pre-edge extrapolation and background removal by a cubic spline method to extract EXAFS oscillations. The EXAFS data were Fourier transformed from *k*-space (30–145 nm⁻¹) to *R*-space. An inverse Fourier transform was performed in a range of 0.09–0.32 nm. The EXAFS parameters were calculated using FEFF code (8.2) for Co–Co, Co–Mo, Co–W, and Co–S atomic pairs.

3. Results

3.1. Catalytic behavior of Co–Mo and Co–W sulfide catalysts supported on SiO₂

Fig. 1 shows the HDS activity of Co/Mo(W)/Si as a function of the presulfidation temperature of Mo(W)/Si. As the presulfidation temperature is increased, the activity increases and then decreases after reaching a maximum at 873 K and 973 K for the Co–Mo and Co–W catalysts, respectively, although the amount of Co accommodated in Co/Mo(W)/Si (as expressed by a Co/Mo(W) atomic ratio) monotonously decreases (Fig. 1). The decrease in the Co/Mo or Co/W atomic ratio is indicative of the decrease in the dispersion of the MoS₂ or WS₂ particles with the increasing sulfidation temperature [22,27,30]. This is also confirmed by the amount of NO adsorption on Mo(W)/Si which is in agreement with a previous study [27]. The surface area and pore size distribution of W/Si are not significantly varied by presulfidation even at 1073 K (BET surface area: 231 m²/g and average pore size: 7.0 nm) compared with those after presulfidation at 673 K (239 m²/g and 7.0 nm, respectively), indicating that the decrease in the dispersions of WS₂ particles and, probably, of MoS₂ particles is not due to the change in the morphology of the support by the thermal treatment. The amount of Mo in Co/Mo/Si did not change after presulfidation below 1073 K under the present sulfidation conditions (XRF analysis).

The turnover frequency (TOF) of the HDS of thiophene on the active sites, Co–Mo(W)–S, of the CVD-catalysts was calculated on the basis of the amount of Co in the catalyst [22]: TOF (h⁻¹) = (activity (mol/g h))/(amount of Co (mol/g)). The reproducibility of TOF thus calculated was better than 10%. Fig. 2 presents the TOF as a function of the presulfidation temperature of Mo(W)/Si. The TOF on Co–Mo–S increases as the temperature is increased up to 873 K, which is in excellent agreement with our previous study [27], and levels off at >873 K, showing the transformation of moderately active Co–Mo–S pseudo Type II [27] to a highly active Co–Mo–S structure. Since the TOF for Co/Mo/Al (13 wt% MoO₃) presulfided at 673 K (TOF for Co–Mo–S Type I by definition [8]) is 7.3 h⁻¹, the TOF of the new Co–Mo–S structure, 16.2 h⁻¹, is about twice as high as that of Co–Mo–S Type I, substantiating the formation of Co–Mo–S Type II on Co/Mo/Si presulfided at >873 K. In our previous study [27], we have attributed

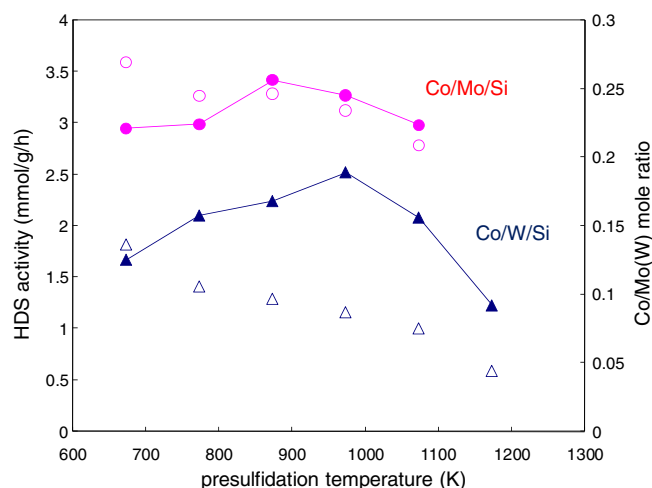


Fig. 1. Catalytic activity of Co/Mo/Si (●) and Co/W/Si (▲) for the HDS of thiophene as a function of the presulfidation temperature. The amount of Co incorporated by the CVD technique is also shown (○: Co/Mo atomic ratio and △: Co/W atomic ratio).

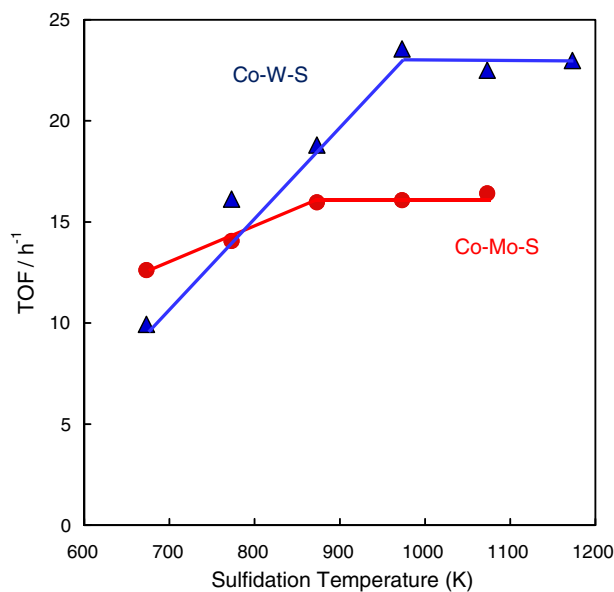


Fig. 2. TOF on SiO₂-supported Co–Mo–S (●) and Co–W–S (▲) as a function of the presulfidation temperature of Mo/Si and W/Si.

the TOF of Co–Mo–S attained at 873 K to the formation of Co–Mo–S Type II without further evidence. Fig. 2 provides a clear evidence for our previous conclusion.

A SiO₂-supported MoS₂ catalyst was prepared by using (NH₄)₂MoS₄ as a precursor to study the effect of MoS₂-support interaction. The HDS activity of Co/Mo/Si (ATM) presulfided at 673 K was 2.7 mmol/g h. The Co content as expressed by a Co/Mo atomic ratio was 0.24, suggesting that the dispersion of MoS₂ particles is slightly lower compared with the oxide-derived catalyst (0.27). The TOF was, thus, calculated to be 16.1 h⁻¹, indicating the formation of Co–Mo–S Type II even at a sulfidation temperature of 673 K.

The TOF on the Co–W–S phase increases more profoundly with the increasing presulfidation temperature of W/Si and levels off at >973 K as shown in Fig. 2. In our previous study [27], we have reported that the TOF on Co–W–S increases up to 873 K. The present study shows a further increase of the TOF by presulfidation at >873 K. The TOF on Co–W–S Type I, 7.1 h⁻¹ for Co/W/Al [27], was almost the same as that on Co–Mo–S Type I (7.3 h⁻¹). In analogy to the formation of Co–Mo–S Type II at >873 K, it is concluded that Co–W–S Type II is formed by presulfidation at >973 K. It is noteworthy that the TOF on Co–W–S remarkably exceeds that on Co–Mo–S at the presulfidation temperature >773 K. In particular, the TOF on Co–W–S Type II is 1.6 times as high as that on Co–Mo–S

Type II. It should be noted that the high TOF of Co–W–S Type II is not due to the contribution of the activity of unpromoted WS₂ particles since W/Si shows only a very low HDS activity (0.12–0.13 mmol/g h).

The reaction products over Mo/Si and W/Si were mainly C₄ compounds with a small amount of propylene regardless of the presulfidation temperature and the addition of Co. The production of a trace amount of butadiene was also detected under the present reaction conditions. The product selectivity, (*n*-butane)/[(*n*-butane) + (butenes)] (mol/mol), was calculated after the reaction time of 1 h to estimate the activity for the hydrogenation of olefins. The results are tabulated in Table 1. The selectivity is considerably increased when Mo/Si is presulfided at >873 K and did not change by the addition of Co. Co/Mo/Si (ATM) (673) shows a selectivity characteristic of Co–Mo–S Type II. The selectivity of Co–W–S is also increased as the presulfidation temperature of W/Si is increased as presented in Table 1.

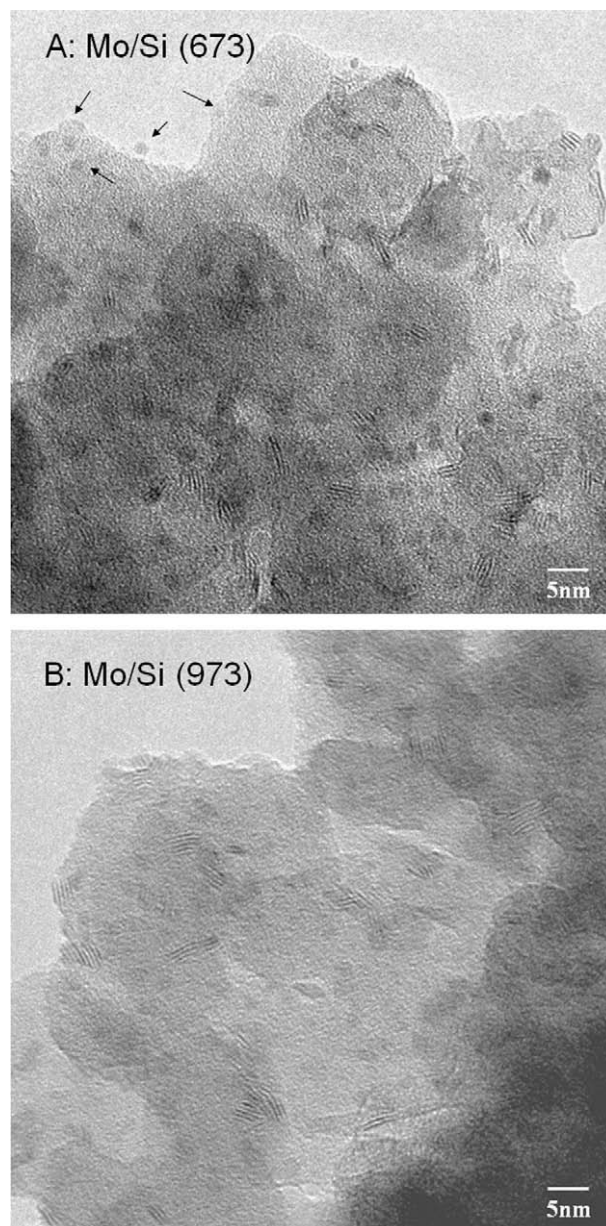


Fig. 3. TEM images of Mo/Si sulfided at 673 K (A) and 973 K (B). Some of the nanosized spot-like entities are indicated by arrows.

Table 1
n-Butane/C₄ selectivity in the HDS of thiophene over SiO₂-supported Co/Mo and Co/W catalysts.

Catalyst	Presulfidation temperature (K)	<i>n</i> -Butane/C ₄ compounds (mol/mol)
Mo/Si	673	0.03
	873	0.14
Co/Mo/Si	673	0.02
	873	0.14
	1073	0.17
Co/Mo/Si (ATM)	673	0.15
Co/W/Si	673	0.05
	873	0.10
	973	0.18
	1073	0.16

3.2. Morphology of MoS₂ particles supported on SiO₂

It is generally believed that the formation of Co–Mo–S Type II is due to the complete sulfidation of Mo and/or the formation of stacked MoS₂ particles [3,6,8–10,16,17,20,21,31]. In the present study, the morphology of MoS₂ particles was observed by TEM. Fig. 3 shows typical TEM images of Mo/Si sulfided at 673 K or 973 K. Well-stacked MoS₂ particles are observed in both samples. However, there are many nanosized spot-like entities in Mo/Si (673) in addition to MoS₂ particles. Reinhoudt et al. [32] and Kooyman et al. [33] have reported the formation of nanosized entities in TEM images for Ni–W/Al₂O₃, and Co–Mo/SiO₂ and Ni–Mo/Al₂O₃, respectively. They assigned these entities to non-crystalline W or Mo (oxy)sulfide particles. In conformity with their assignments, we can hardly find these entities in Mo/Si (973) (Fig. 3). The distributions of size and stacking number of MoS₂ particles calculated

Table 2
TEM analysis of Mo/Si catalysts sulfided at 673 K and 973 K.

Particle size (nm)	Fraction of particles (%)	
	673 K	973 K
0–2	35.4	21.5
2–4	49.5	59.5
4–6	13.5	14.8
6–8	1.0	3.2
8–10	0.6	1.0
Average size (nm)	2.69	3.06
Number of stacking	673 K	973 K
1	27.8	20.4
2	30.5	25.0
3	23.9	25.7
4	9.4	12.0
5	5.9	7.1
6	1.7	4.9
≥7	0.8	4.9
Average number of stacking	2.43	2.95

from the TEM images and their average values are summarized in Table 2. The size and stacking number of MoS₂ particles are increased by the increase in the presulfidation temperature, as expected, but the changes are not very significant.

3.3. Sulfidation behavior of SiO₂-supported Mo and W oxides

The sulfidation behavior of MoO₃/SiO₂ and WO₃/SiO₂ was studied by using a TPS technique. Fig. 4 presents the TPS profiles of MoO₃/SiO₂. The H₂S consumption pattern has both characteristics of the profiles reported by Scheffer et al. [34] for MoO₃/SiO₂ samples with 3.5 wt% and 35 wt% MoO₃. Judging from their study, it is considered that the sulfidation of MoO₃ starts with the O–S exchange to form MoO_{3–x}S_y (<450 K, region I), followed by H₂-reduction to MoS_{2–x}O_y at 480 K and subsequent sulfidation to MoS₂ (>500 K, region II). A considerable H₂S consumption in “region II” shown in Fig. 4 indicates the presence of MoO₃ crystallites, which is sulfided via MoO₂ because of diffusion limitations [34,35], together with highly dispersed Mo oxides. Fig. 4 shows that the sulfidation of Mo oxides is not completed at 673 K and that the H₂S consumption continues until 873 K, accompanying a slight H₂ consumption around 700 K. It is concluded that the sulfidation of Mo oxides to MoS₂ is completed above 873 K for the present MoO₃/SiO₂.

Fig. 5 shows the TPS profiles of WO₃/SiO₂. Judging from the TPS profile for crystalline MoO₃ [34,35], the TPS shows the predominant presence of WO₃ crystallites. The H₂S consumption pattern shows that the sulfidation of W oxides is completed at >950 K. The TPS profiles shown in Figs. 4 and 5 clearly demonstrate that the temperatures of the complete sulfidation of Mo and W oxides to MoS₂ and WS₂ correspond to the temperatures of the formation of Co–Mo–S Type II and Co–W–S Type II, respectively.

3.4. Magnetic property of Co–Mo–S

In our previous study [27,29,36], we have revealed that the Co atoms in Co–Mo–S show antiferromagnetic properties and that

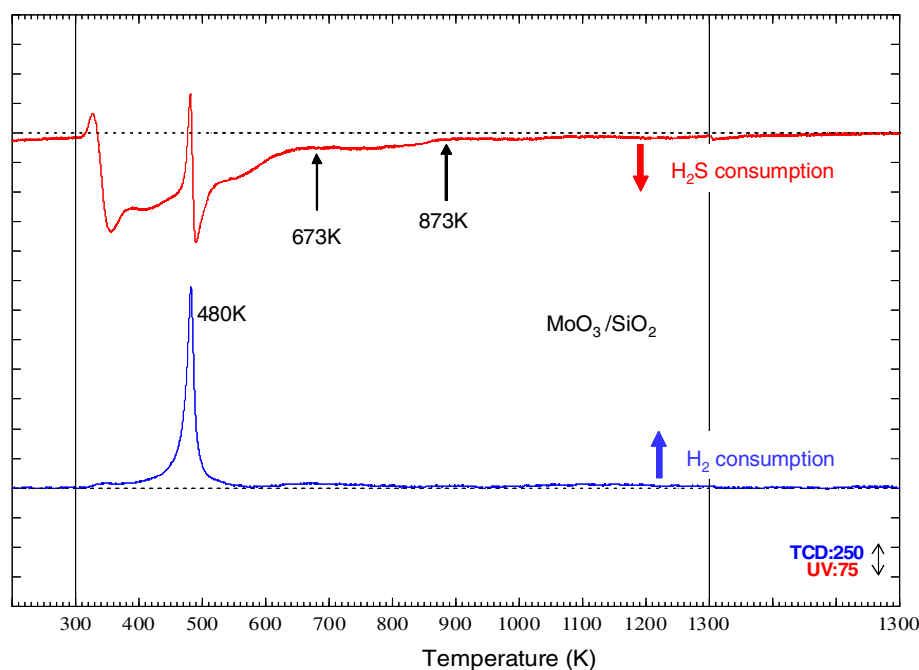


Fig. 4. TPS profiles of 10 wt% MoO₃/SiO₂.

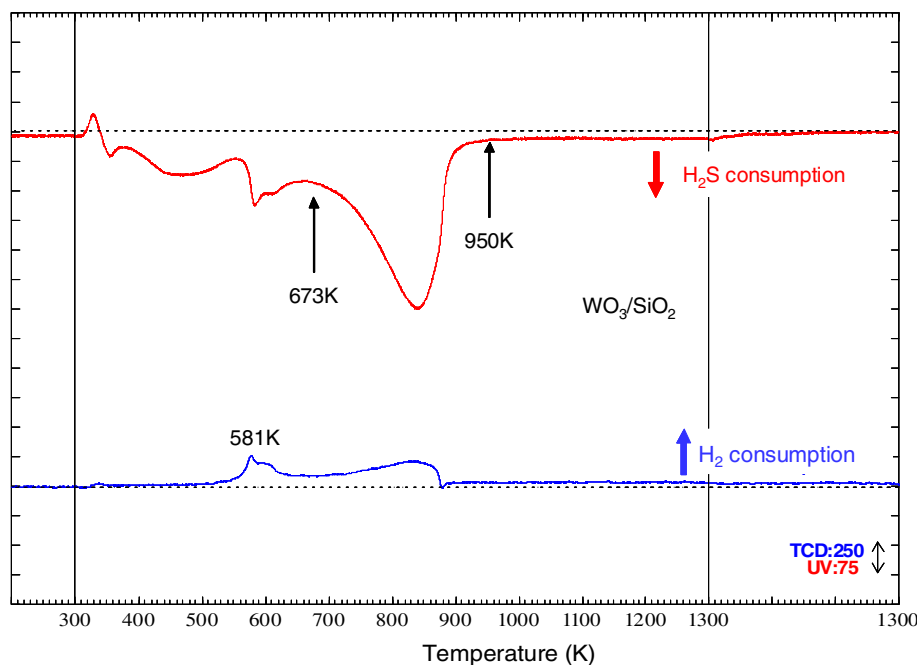


Fig. 5. TPS profiles of 20 wt% WO_3/SiO_2 .

the temperature dependence of magnetic susceptibility of Co is simulated by a theoretical equation (1) [37] for dinuclear Co sulfide clusters

$$\chi = \alpha N_A g^2 \mu_B^2 / k_B T [3 + \exp(-2J/k_B T)] \quad (1)$$

where N_A is Avogadro's constant, μ_B is Bohr magneton, g is the gyromagnetic factor (assumed to be 2 here), k_B is Boltzmann's constant, J is the magnetic interaction strength defined by $H = -2J\mathbf{S}_1 \cdot \mathbf{S}_2$, and α is the fraction of the paramagnetic spin per Co atom. In our previous experiments [27,29], we measured the magnetic properties of Co/Mo catalysts using a Pyrex glass tube or a quartz glass tube. However, when a Pyrex glass tube was used, the magnetic moment of the tube itself was very large and then it was found that the accuracy of the value of J was thereby reduced. Accordingly, in the present study, we decided to systematically measure the magnetic properties of Co/Mo catalysts again using a quartz glass tube.

Fig. 6 shows the representative results of magnetic measurements for Mo and Co/Mo catalysts. Mo/B–Al shows weak magnetic susceptibility possibly due to Mo^{5+} species. The number of spins was calculated to be 0.02–0.03/Mo, an order of magnitude lower than the amount of Co. On the other hand, Co/Mo/B–Al exhibits much stronger magnetic susceptibility, negating the possibility that the antiferromagnetic behavior of Co is caused by an interaction between a single spin of Co and a single spin of MoS_2 particles due to the coordinative unsaturation of their edges [38]. The magnetic susceptibility of Co was extracted by subtracting the magnetic susceptibility of Mo/B–Al from that of Co/Mo/B–Al. Fig. 6 also presents the magnetic susceptibility of Co thus obtained for Co/Mo/B–Al, distinctly demonstrating an antiferromagnetic behavior of Co. All the catalysts examined in the present study show antiferromagnetic properties, confirming the previous results [27,29,36]. The $-2J$ values obtained using Eq. (1) are summarized in Table 3 for Co/Mo/Si (20 wt% MoO_3) sulfided at 673 K and 873 K, Co/Mo/B–Al catalysts with varying boron contents, and Co/Mo/Al. All these catalysts were prepared by the CVD technique. The $-2J$ value for Co/Mo/Si (10 wt% MoO_3), which has been measured previously using a quartz glass tube [27], is included in Table 3. The accuracy of the relative $-2J$ value is estimated to be within

± 0.5 K. It is noteworthy that the $-2J$ value varies with the support and the sulfidation temperature.

The relative TOF values on the catalysts taken from our previous reports [13,27] are also summarized in Table 3. Fig. 7 shows the TOF value relative to that on Co–Mo–S Type I as a function of $-2J$ value. It is evident that the relative TOF is correlated well with the $-2J$ value and that as the $-2J$ value increases, the TOF increases from Co–Mo–S Type I for Co/Mo/Al (673) to Co–Mo–S Type II for Co/Mo/Si (873). It is concluded that Co–Mo–S Type I and Type II can be differentiated by the magnetic property.

3.5. EXAFS analysis of Co–Mo–S and Co–W–S

The local structure of Co–Mo–S was reported to depend on the support and type (or TOF) [10,39]. We studied the structure of Co–Mo–S using Co K-edge XAFS for the Co/Mo catalysts to explore the effects of the support (SiO_2 vs. Al_2O_3) and sulfidation temperature. Fig. 8 shows the Co K-edge XANES spectra for Co/Mo/Si and Co/Mo/Si (ATM). The XANES spectra for Co/Mo/Al and Co/Al, which was prepared by exposing Al_2O_3 to a vapor of $\text{Co}(\text{CO})_3\text{NO}$ and then sulfided, have been reported elsewhere [40], but the spectrum of Co/Mo/Al (673) is included in Fig. 8 for clarity. The 1s–3d preedge peak intensity around 7707 eV for the SiO_2 -supported catalysts is considerably lower than that for a reference compound Co_9S_8 , indicating that the Co atoms in Co–Mo–S are in a higher symmetry than tetrahedral, which is in agreement with other works done on Co–Mo–S [10,39]. The XANES spectra are very close to one another, but the shoulder peaks around 7720 eV of Co/Mo/Si (873) and Co/Mo/Si (ATM) (673) are prominent than those of Co/Mo/Al (673). Co/Mo/Si (673) exhibits an intermediate spectral feature. The slight but distinct difference in the XANES spectra suggests the different electronic state and/or local structure of Co–Mo–S among these catalysts.

Fig. 9 presents the $k^3\chi(k)$ EXAFS oscillations and their Fourier transforms for Co/Mo/Al and Co/Mo/Si. The Fourier transform of Co/Al is also shown in Fig. 9 for comparison. Co/Al shows one intense peak at 0.18 nm with a shoulder peak around 0.23 nm (phase shifts: uncorrected). However, the Co/Mo catalysts, in particular,

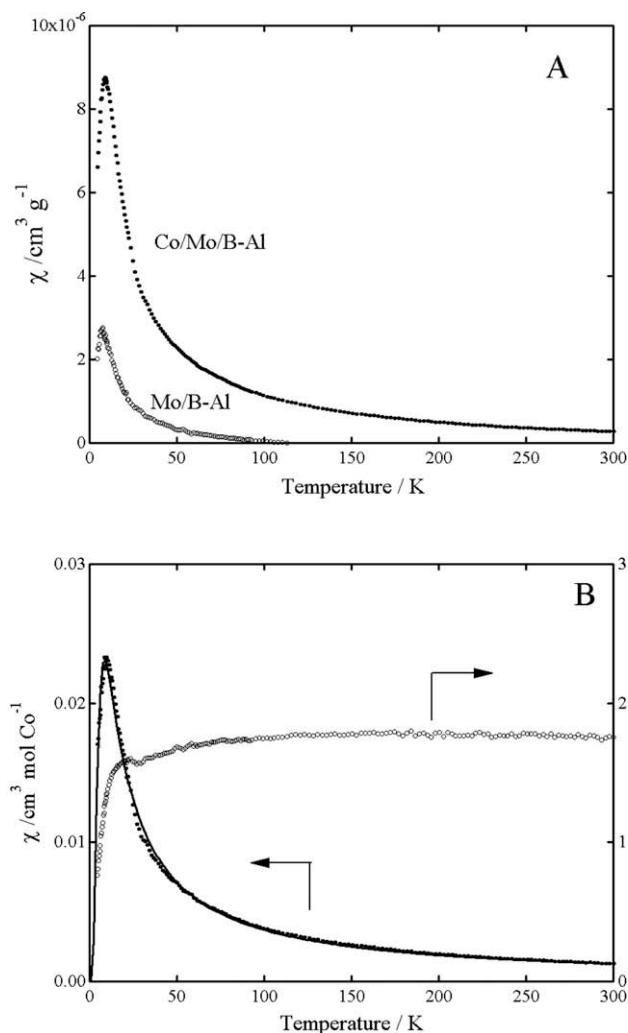


Fig. 6. (A) Magnetic susceptibilities of Mo/B-Al (0.6% B) and Co/Mo/B-Al (0.6% B) as a function of temperature, (B) magnetic susceptibility, and effective magnetic moment of Co in Co/Mo/B-Al (0.6% B) against temperature. The best fitting curve, assuming a dinuclear cluster, for the observed magnetic susceptibility is also shown.

Co/Mo/Si show well-resolved three shells around 0.18, 0.24, and 0.28 nm (phase shifts: uncorrected) in the Fourier transforms. Obviously, the presence of MoS₂ particles results in the formation of Co sulfide species with a local structure that is distinctly different from that of Co sulfide clusters on Al₂O₃, which is in agreement with XPS [22]. It is worth noting that the Co K-edge Fourier transforms shown in Fig. 9 are better resolved than those reported by Bouwens et al. [10,39] since we can adopt a wider range of k (30–145 nm⁻¹) than theirs (28–101 nm⁻¹), which was limited by Ni contamination in Co. This is one of the merits of using Co(CO)₃NO as a precursor to Co sulfide.

The Fourier transform for Co/Al was analyzed using FEFF parameters, assuming Co–S and Co–Al atomic pairs. The structural parameters are presented in Table 4. The crystallographic data of Co₉S₈ are also presented for comparison [41]. The atomic distances of Co–S and Co–Co are in good agreement with those of Co₉S₈. The coordination number (CN) of Co–Co is considerably smaller than that of Co₉S₈, while CN of Co–S is almost the same as that of the reference compound. Evidently, the EXAFS analysis shows the formation of small Co₉S₈-like Co sulfide clusters in Co/Al, which is in excellent agreement with the previous XPS analysis [22]. These results may substantiate that the present EXAFS analysis is reasonable.

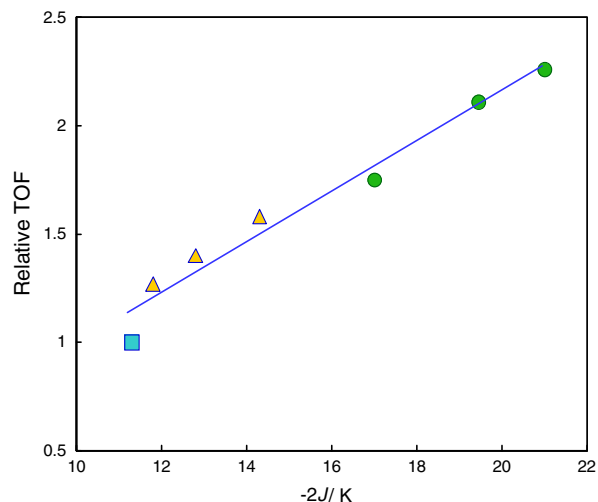


Fig. 7. Correlation between relative TOF of Co–Mo–S and magnetic parameter $-2J$. Support and presulfidation temperature: square, Al₂O₃ (673 K); triangle, B₂O₃–Al₂O₃ (0.3–2.5 wt% B); and circle, SiO₂ (673–873 K). See Table 3 for details.

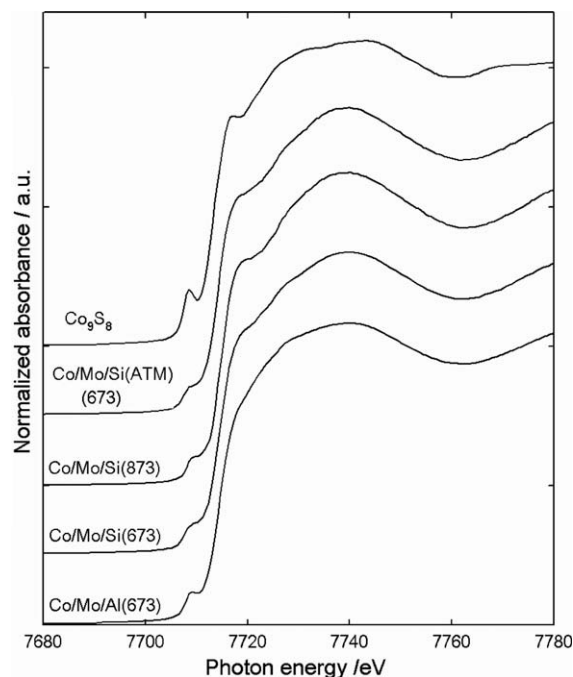


Fig. 8. Co K-edge XANES spectra for Co/Mo/Al (673), Co/Mo/Si (673), Co/Mo/Si (873), Co/Mo/Si (ATM) (673), and Co₉S₈.

The Fourier transform for Co/Mo/Al (673) was analyzed, assuming three shells of Co–S, Co–Mo, and Co–Co atomic pairs at increasing atomic distances, respectively. The structural parameters obtained are summarized in Table 4. The atomic distance of Co–S (0.221 nm) is very close to the values reported by other groups for Al₂O₃-, SiO₂-, and C-supported Co–Mo catalysts [10,39,42]. The atomic distance of Co–Mo (0.280 nm) is slightly shorter than the values (0.281–0.289 nm) reported by Bouwens et al. [10,39]. The Co–Co atomic distance is 0.313 nm and is slightly shorter than the Mo–Mo atomic distance of MoS₂ (0.316 nm). The CN of the Co–Co shell is close to unity.

The Fourier transforms for Co/Mo/Si presulfided at 673 K and 873 K and for Co/Mo/Si (ATM) were analyzed in a manner similar to that used for analyzing the Al₂O₃ counterpart. The structural

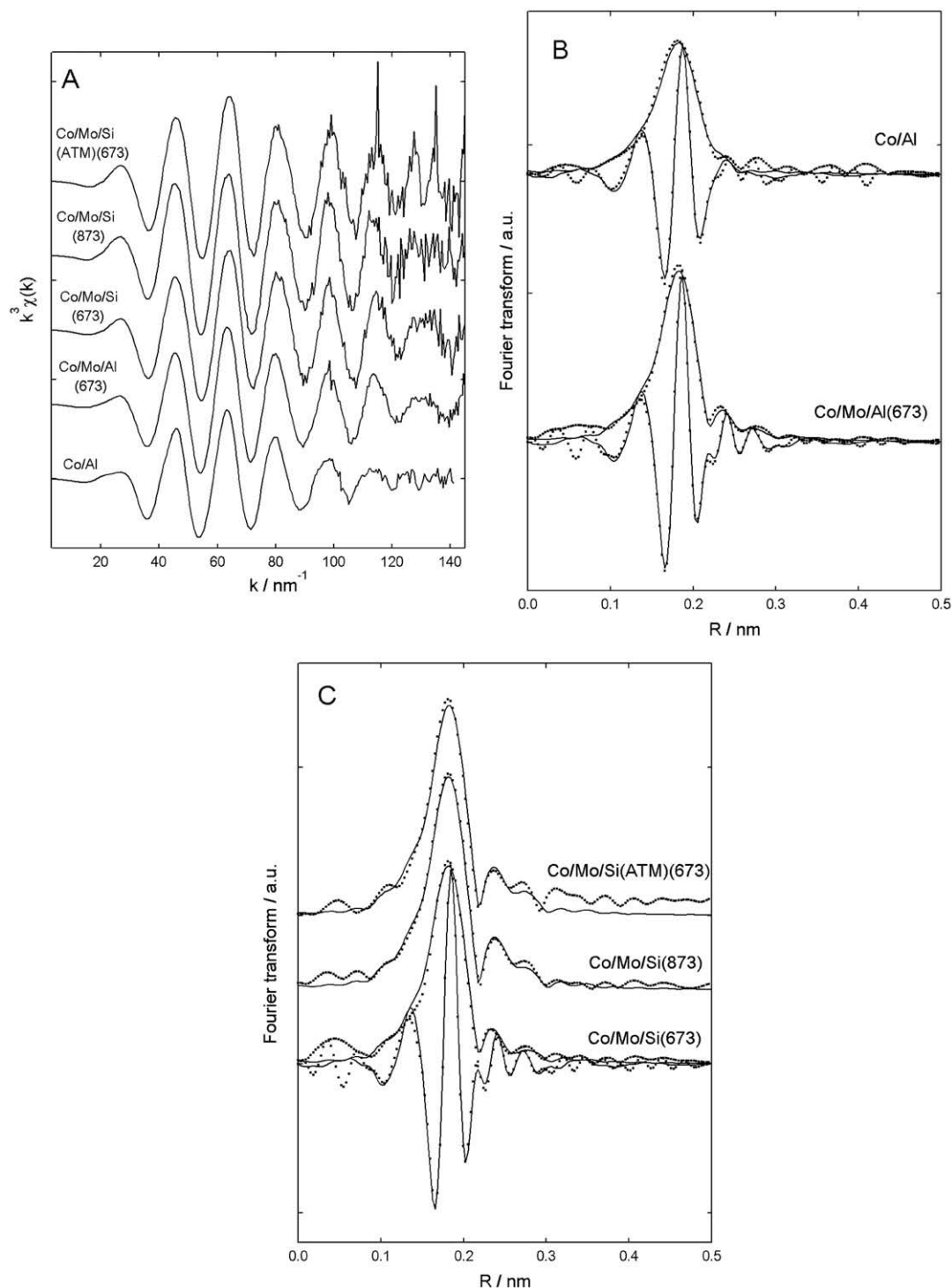


Fig. 9. $k^3\chi(k)$ EXAFS oscillations (A) and corresponding Fourier transforms (B and C). (A) Co/Al, Co/Mo/Al (673), Co/Mo/Si (673), Co/Mo/Si (873), and Co/Mo/Si (ATM) (673). (B) Co/Mo/Al (673) and Co/Al; and (C) Co/Mo/Si (673), Co/Mo/Si (873), and Co/Mo/Si (ATM) (673). Dots: observed Fourier transforms, and solid line: best curve-fittings.

parameters are summarized in Table 4. The structural parameters are not significantly affected by the support, presulfidation temperature, and preparation method, suggesting that the local structure of Co–Mo–S is essentially the same regardless of the preparation parameters. Nevertheless, it should be noted that there are small but clear tendencies of a shorter Co–S atomic distance (0.220 nm), a longer Co–Co atomic distance (0.315 nm), and smaller Debye–Waller-like parameters for Co–Mo–S Type II compared

with those for Type I. In addition, it is evident that the CNs of Co–S for Co/Mo/Si (873) and Co/Mo/Si (ATM) (673) (Co–Mo–S Type II) are higher than that of Co/Mo/Al (673) (Type I). No direct Co–O–support interaction was detected in the EXAFS analysis of the present Co/Mo catalysts.

Fig. 10 shows the Co K-edge Fourier transforms of k^3 -weighted $\chi(k)$ for Co/W/Al and Co/W/Si presulfided at 673 K. Co/W/Si (673) shows well-resolved three shells, which are assigned to Co–S,

Table 3
Relative TOF and $-2J$ values for Co/Mo catalysts supported on Al₂O₃, B₂O₃-Al₂O₃, and SiO₂.

Catalyst					$-2J$ (K)	Relative TOF ^a
Support	MoO ₃ content (wt%)	Boron content (wt%)	Presulfidation temperature (K)	Co content (wt%)		
Al ₂ O ₃	13		673	2.65	11.2	1.0
B ₂ O ₃ -Al ₂ O ₃	13	0.3	673	2.45 ^b	11.8	1.27 ^b
		0.6	673	2.33 ^b	12.8	1.40 ^b
		2.5	673	1.54 ^b	14.3	1.58 ^b
SiO ₂	10		673	1.10	17.0 ^c	1.75
	20		673	0.76 ^c	19.4	2.11 ^c
	20		873	0.65 ^c	21.0	2.26 ^c

^a TOF relative to the value for Co/Mo/Al presulfided at 673 K.

^b Previous results [13].

^c Previous results [27].

Table 4
Structural parameters^a derived from Co K-edge EXAFS analysis of Co/Mo/Al, Co/Mo/Si, and Co/Al catalysts.

Catalyst (presulfidation temp.)	Atomic pair	CN	R (nm)	ΔE_0 (eV)	σ (10 ⁻³ nm)	R _f (%)
Co/Mo/Al (673 K)	Co-S	4.2	0.220 ₈	1.0	8.7	0.9
	Co-Mo	1.5	0.280 ₃	3.9	11.3	
	Co-Co	0.7	0.313 ₀	-7.9	11.8	
Co/Mo/Si (673 K)	Co-S	4.5	0.219 ₅	1.1	8.4	1.3
	Co-Mo	1.5	0.281 ₀	3.9	11.3	
	Co-Co	0.8	0.314 ₇	-8.1	11.7	
Co/Mo/Si (873 K)	Co-S	4.9	0.220 ₀	0.6	8.3	1.0
	Co-Mo	1.6	0.282 ₉	3.2	9.5	
	Co-Co	1.0	0.314 ₇	-8.1	10.6	
Co/Mo/Si (ATM) (673 K)	Co-S	4.7	0.219 ₈	2.2	8.2	0.6
	Co-Mo	1.5	0.280 ₈	3.3	9.8	
	Co-Co	0.9	0.314 ₉	-7.6	9.6	
Co/Al (673 K)	Co-S	4.1	0.221 ₁	0.0	9.9	1.7
	Co-Co	0.6	0.251 ₂	-3.4	11.8	
Co ₉ S ₈ ^b	Co-S	4.2	0.2227	-	-	-
	Co-Co	2.7	0.2505	-	-	

^a CN, coordination number; R, distance; E₀, inner potential; σ , Debye-Waller-like factor; and R_f, R factor defined as $R_f = \left\{ \frac{\sum [\chi_{\text{obs}}(k) - \chi_{\text{cal}}(k)]^2}{\sum \chi_{\text{obs}}(k)^2} \right\}^{1/2}$.

^b Average crystallographic parameters of Co₉S₈.

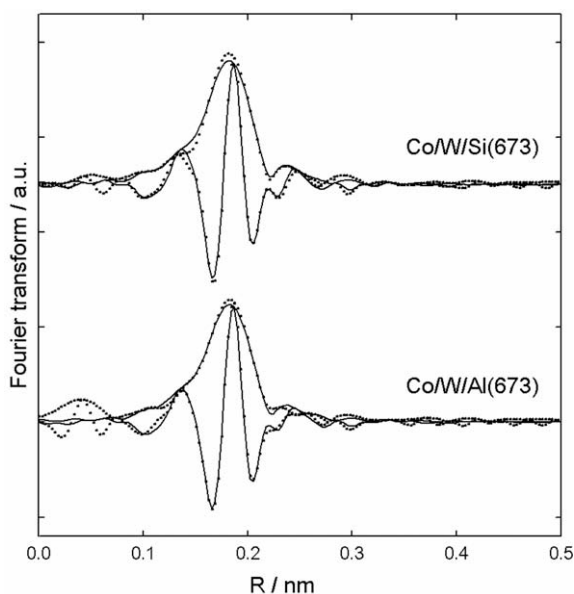


Fig. 10. Fourier transforms of $k^3\chi(k)$ Co K-edge EXAFS oscillations for Co/W/Al and Co/W/Si presulfided at 673 K.

Table 5
Structural parameters^a derived from Co K-edge EXAFS analysis of Co/W/Al and Co/W/Si.

Catalyst (presulfidation temp.)	Atomic pair	CN	R (nm)	ΔE_0 (eV)	σ (10 ⁻³ nm)	R _f (%)
Co/W/Al (673 K)	Co-S	4.5	0.220 ₉	1.5	8.7	0.8
	Co-W	0.9	0.278 ₄	7.0	11.4	
	Co-Co	0.3	0.314 ₈	-8.2	12.3	
Co/W/Si (673 K)	Co-S	4.5	0.220 ₈	0.3	8.4	1.5
	Co-W	1.3	0.277 ₂	8.6	11.0	
	Co-Co	0.6	0.315 ₃	-8.6	11.6	

^a CN, coordination number; R, distance; E₀, inner potential; σ , Debye-Waller-like factor; and R_f, R factor defined as $R_f = \left\{ \frac{\sum [\chi_{\text{obs}}(k) - \chi_{\text{cal}}(k)]^2}{\sum \chi_{\text{obs}}(k)^2} \right\}^{1/2}$.

Co-W, and Co-Co atomic pairs at increasing distances. Table 5 presents the structural parameters obtained from the EXAFS analysis using FEFF parameters. The structural parameters for Co-W-S are essentially identical to those for Co-Mo-S. The CN and atomic distance of the Co-Co contribution for Co-W-S are suggestive of the presence of a Co sulfide dinuclear structure on the edge of WS₂ particles, which is in agreement with the antiferromagnetic behavior of Co-W-S [27].

4. Discussion

4.1. Formation of Co–Mo–S Type II

Fig. 2 demonstrates that Co–Mo–S Type II is formed when Mo/Si is presulfided at >873 K. Since the sulfidation temperature of Co/Mo/Si is fixed at 673 K after the addition of Co using the CVD method, it is concluded that the formation of Co–Mo–S Type II is elucidated by the presulfidation temperature of Mo/Si and, hence, that the intrinsic activity of Co–Mo–S is determined by the chemical and/or electronic properties of MoS₂ particles, which is in agreement with the EXAFS results showing the absence of direct interactions between Co and the support. The present results substantiate that there is no need to increase the treatment temperature of Co–Mo–S itself for the formation of Co–Mo–S Type II. Instead, when Co–Mo–S was treated in H₂S/H₂ or in vacuum at >673 K, a partial destruction of Co–Mo–S was observed by Usman et al. [43].

The TPS profiles shown in Fig. 4 and the TEM observations shown in Fig. 3 lead us to conclude that the catalytic properties are predominantly controlled by the sulfidation degree of Mo. When the sulfidation of Mo oxide precursors is incomplete, MoS_xO_y nanosized entities and MoS₂–O–support interaction species remain on the catalyst surface. Mo oxide–O–SiO₂ interactions have been envisaged by de Boer et al. [44] and Iwasawa [45]. Judging from the sulfidation mechanism [34,35], the TPR profile also suggests the possibility of MoS₂–O–MoO₂ linkages between surface MoS₂ particles and MoO₂ cores. All these Mo sulfide–oxygen bonds may modify the chemical nature of Mo sulfides. Hinnemann et al. [17] suggested using DFT calculations that the Mo–S bonds in MoS₂ are strengthened by MoS₂–O–support interactions, thus reducing the reactivity. Their DFT calculations also suggest that the electronic state of MoS₂ particles is strongly affected by the Mo–O bonds, leading to unclear one-dimensional metallic states, BRIM sites. The DFT calculations by Arrouvel et al. [18] and Costa et al. [19] suggest that MoS₂–O–support interactions are prominent for small MoS₂ particles such as Mo₆S_x under usual sulfidation and HDS conditions. They have also shown that parallel orientation of MoS₂ particles to the support surface becomes stable because of van der Waals forces and hydrogen bonding with surface hydroxyl groups. Their DFT results may account for the formation of Co–Mo–S Type I in Co/Mo/Al, in which MoS₂ particles are highly dispersed.

The present TPS profiles shown in Fig. 4 clearly substantiate the idea that complete sulfidation of Mo, that is, the formation of MoS₂ particles without any chemical bonds with the support and, instead, with van der Waals forces and possibly weak hydrogen bonding with surface hydroxyl groups alone is a prerequisite for the formation of Co–Mo–S Type II. This is also supported by the findings that Co–Mo–S Type II is formed even at the presulfidation temperature of 673 K for Co/Mo/Si (ATM), in which thiomolybdate had been used as a precursor and thus the formation of MoS₂–O–SiO₂ or –MoO₂ linkages may be suppressed very much. The removal of the interaction of MoS₂ with the support surface accompanies the sintering of MoS₂ particles and the increase in the stacking number (Fig. 3 and Table 2). The TOF of the HDS of thiophene may not be geometrically influenced by the increased stacking number of Co–Mo–S because of a rather small molecular size. Eijsbouts et al. [31] suggested the formation of Type II active sites without stacking of MoS₂ particles in industrial catalysts.

In Table 1 the hydrogenation activity of the Mo and Co/Mo catalysts during the HDS of thiophene is given. Evidently, the hydrogenation activity is increased by the formation of Co–Mo–S Type II. Co/Mo/Si (ATM) shows characteristics of Co–Mo–S Type II in spite of a low sulfidation temperature. It is considered that weaker Mo–S and, possibly, Co–S bond strengths [17] in the Type II forms may facilitate the formation of coordinatively unsaturated sites for

the hydrogenation. In addition, the high hydrogenation selectivity of Co–Mo–S Type II may also be correlated with the full development of BRIM sites [46] on the periphery of the (0001) basal surface of MoS₂ particles as claimed by Hinnemann et al. [17]. By means of STM, Lauritsen et al. [47] and Topsøe [48] suggested that the hydrogen addition to thiophene is promoted on BRIM sites for MoS₂/Au(111). In line with this, Daage and Chianelli [49] have proposed a “Rim-Edge” model to explain the HDS-hydrogenation selectivity of MoS₂ catalysts. We can reach the same conclusion for the Co/W catalysts from Table 1.

Recent theoretical calculations using DFT predict that the local structure and location of Co–Mo–S, the coverage of Co on the MoS₂ edge, and the morphologies of MoS₂ and Co–MoS₂ particles (metal-edge/sulfur-edge ratio) depend on the P_{H₂S}/P_{H₂} ratio and temperature, that is, the chemical potential of sulfur ($\Delta\mu_s$) of the reaction system under the sulfidation and reaction conditions [50,51]. Hence, it is easily expected that the intrinsic activity of Co–Mo–S is determined by the preparation and reaction conditions of Co–MoS₂ catalysts as well as by the interactions of MoS₂ and the support. As a consequence, it should be noted that Co–Mo(W)–S Type II is defined as the Co–Mo(W)–S structure without strong interactions with the support and that the intrinsic activity of Co–Mo(W)–S Type II depends on the reaction conditions that determine the $\Delta\mu_s$ value of the reaction system.

4.2. Intrinsic activity of Co–W–S Type II

The TPS profiles shown in Fig. 5 prompt us to conclude that Co–W–S Type II is formed only when W oxides are completely sulfided to WS₂ particles. The formation of Co–W–S pseudo Type II with a TOF intermediate between Type I and Type II has been reported for Co/W/B–Al catalysts with varying boron contents, as observed for Co–Mo counterparts [14], indicating that the intrinsic activity of Co–W–S is dependent on the interaction between WS₂ particles and support surface.

Fig. 2 clearly demonstrates that Co–W–S Type II has a much higher intrinsic activity than Co–Mo–S Type II, while Co–W–S Type I has an activity similar to that of Co–Mo–S Type I. Since the edges of MoS₂ and WS₂ particles are fully occupied by the Co atoms forming Co–Mo(W)–S in the CVD-catalysts [22,40], the lower HDS activity of Co/W/Si shown in Fig. 1 is apparently ascribed to a lower dispersion of WS₂ particles than of MoS₂ particles, as evidenced by smaller amounts of Co accommodated in the catalysts (Co/W atomic ratio \ll Co/Mo atomic ratio), which is in good agreement with NO adsorption capacity reported previously [30].

Chianelli et al. [52] and Chianelli [53] proposed a volcano-type correlation between the (average) heat of formation of metal sulfides and their specific HDS activity (activity/surface area). They predicted that a Co–WS₂ catalyst might be as active as or even more active than a Co–MoS₂ catalyst. In contrast, Raybaud et al. [50,54,55] suggested a lower HDS activity of Co–W–S than of Co–Mo–S on the basis of the theoretical sulfur metal bond energy at the edge, assuming 50% coverage of Co. As mentioned above, it is deduced from recent DFT calculations [50,51] that the intrinsic activity of Co–Mo–S depends on the local structure and location (metal-edge or sulfur-edge). Very recently, Gandubert et al. [56] suggested on the basis of a combined theoretical and experimental study that Co–Mo mixed sites on the metal-edge show a considerably higher activity than Co–Mo–S on the sulfur-edge for the hydrogenation of toluene. Their results may suggest that the intrinsic activity of Co–Mo(W)–S depends on their location. Besides, it is well documented that the fractions of the metal-edge and sulfur-edge of Co–MoS₂ particles depend on the $\Delta\mu_s$ value [50,57,58]. In the present study, the TOF values are averaged over those of Co–Mo(W)–S on the metal- and sulfur-edges (*vide infra*).

Hence, the higher TOF of Co–W–S may be due to a higher fraction of the more favorable edge (for instance, metal-edge [56]) of Co–WS₂ particles and/or to a greater intrinsic activity difference between the Co–W–S structures on these edges and/or to more favorable electronic states of Co–W–S compared to Co–Mo–S.

It is generally accepted that Co–W sulfide catalysts exhibit a much lower HDS activity than Co–Mo counterparts [4]. One of the reasons is a lower sulfidation degree of W than of Mo because of a higher difficulty in the sulfidation of W oxides supported on Al₂O₃ than of Mo oxides [3,4]. Another reason is the lower coverage of Co on the edge of WS₂ particles because of a much greater difference of the sulfidation temperatures of Co and W in comparison with that between Co and Mo. Kishan et al. [24] and Kubota et al. [26] showed that the use of a chelating agent considerably increases the sulfidation temperature of Co by a complex formation with the chelating agent, leading to a great HDS activity increase of Co–WS₂ catalysts. In addition, it should be noted that WS₂ particles are apt to sinter when WS₂–O–support interactions are absent as shown in Fig. 1 and in our previous study [30]. Nevertheless, it is expected that Co–WS₂ catalysts could show a higher HDS activity than Co–MoS₂ catalysts if the former catalysts were properly prepared by a sophisticated preparation procedure.

4.3. Effects of the support and presulfidation temperature on the intrinsic activity of Co–Mo–S

The interaction between MoS₂ particles and the support is controlled by the presulfidation temperature. With increasing presulfidation temperature, stronger Mo–O–support bonds are progressively sulfided to form MoS₂ particles, leaving a smaller amount of such unfavorable linkages. On the other hand, the addition of boron or phosphorus removes surface basic hydroxyl groups of the support [11–14], thus preventing strong Mo–O–support interactions. In this sense, it is considered that the effects of the support and presulfidation temperature can be discussed in terms of the same parameter. This is substantiated by a single correlation shown in Fig. 7 between the TOF and $-2J$ value for the catalysts prepared by the use of different supports and presulfidation temperatures (Table 3). The magnetic parameter J represents the interaction strength between two Co atoms in Co–Mo–S dinuclear clusters through the Co–S–Co bond, that is, the electronic state of Co–Mo–S, which is considered to be modified by the electronic state of MoS₂ particles which is determined by the support and presulfidation temperature via MoS₂–O–support linkages. It is considered that the change of the electronic state of Co–Mo–S, which may be closely correlated with the change in its local structure, results in the change of intrinsic activity through modifying, for instance, the Co–S bond energy. It is worth noting in Fig. 7 that the magnetic property of Co–Mo–S differentiates Co–Mo–S Type I and Type II.

According to the DFT calculations by Raybaud et al. [50,59], the sulfur metal bond energy decreases as the coverage of Co on the MoS₂ edge increases. This may suggest that the intrinsic activity of Co–Mo–S for HDS is varied by the Co content at the edge, as noted by Raybaud [50]. The magnetic property of Co–Mo–S may provide some suggestions for this issue. We have reported the J value of Co–Mo–S for Co–Mo/Al₂O₃ (13 wt% MoO₃) catalysts prepared by an impregnation technique as a function of Co content [36]. The $-2J$ value increased from 10.0 K to 11.2 K as the amount of Co increased from Co/Mo = 0.14 to 0.58. The $-2J$ value for the impregnation catalysts with Co/Mo = 0.43–0.58 agrees very well with the value for Co/Mo/Al (Co/Mo = 0.50) having a full coverage of Co (Table 3). The $\Delta(-2J)$ value (1.2 K) corresponds to 12% of the difference between Co–Mo–S Type I and Type II, assuming a linear correlation in Fig. 7. Accordingly, it is estimated that when

the Co content on the MoS₂ edge increases from 0.11 (corrected for α in Eq. (1)) to 0.50 (full coverage), the relative TOF of Co–Mo–S is increased by 0.15 in Fig. 7 compared with the increase of 1.26 for the transformation of Type I to Type II. As suggested by Raybaud [50], the intrinsic activity of Co–Mo–S will be varied by the Co coverage on the edge, but the magnitude of the change is expected not to be very significant. This expectation may be supported by linear relationships between HDS activity and the amount of Co–Mo–S reported by several groups [8,11,21,60]. It is considered that the relatively small change in the intrinsic activity of Co–Mo–S with the Co coverage is associated with the findings that Co–Mo–S has a dinuclear Co sulfide structure regardless of the Co content on the MoS₂ edge instead of a single-Co atom structure with a Co–S–Mo linkage [39] as discussed below (4.4).

4.4. Structure of Co–Mo–S

The elucidation of the local structure of Co–Mo–S is of great importance to understand the adsorption and catalysis on HDS catalysts. The present EXAFS analysis of the Co/Mo catalysts clearly shows the presence of Co–Co scattering together with Co–S and Co–Mo shells. The CN of Co–Co contribution is close to unity, substantiating the formation of dinuclear Co sulfide clusters on the edge of MoS₂ particles, which is in excellent agreement with the antiferromagnetic property of Co–Mo–S. Structural models of Co–Mo–S, satisfying the EXAFS parameters given in Table 4, can be constructed for both (10 $\bar{1}$ 0) Mo-edge and ($\bar{1}$ 010) S-edge of MoS₂ particles. Plausible models are presented in Fig. 11. The model on the Mo-edge is very close to the theoretical model proposed by Raybaud et al. [59] as an energetically favorable structure for a Mo-edge fully promoted by Co. Very recently, using DFT calculations in conjunction with thermodynamics, Krebs et al. [58] suggested a Co sulfide dinuclear structure on a S-edge with a 100% coverage of Co and a Co–Co pair configuration on a Mo-edge with a 50% coverage of Co. The magnetic study of Co–Mo/Al₂O₃ catalysts prepared by an impregnation method showed the formation of dinuclear Co sulfide clusters even at a low content of Co–Mo–S [36]. From their EXAFS analysis, Bouwens et al. [10,39] proposed a single-Co atom model for Co–Mo–S, in which the Co atom is in a square pyramidal configuration on the edge of MoS₂. We have previously pointed out that the dinuclear cluster model explains the NO adsorption capacity of Co–Mo–S [29,61] as well as the magnetic property [29]. It is interesting to note here that Louwers and Prins [62] found a Ni–Ni contribution with an atomic distance of 0.315–0.323 nm and a CN of around unity in their EXAFS analysis of Ni–Mo–S. They assigned the Ni–Ni contribution to scattering due to a Ni atom adjacent to the square pyramidal Ni atom constituting Ni–Mo–S, but the formation of dinuclear Ni sulfide clusters on the edge of MoS₂ particles may account for their EXAFS structural parameters.

The structural parameters for Co–W–S given in Table 5 suggest the formation of a dinuclear Co sulfide structure on the edge of WS₂ particles in agreement with the antiferromagnetic interactions between the Co atoms [27]. These results suggest that the structural models shown in Fig. 11 are applicable to Co–W–S too.

The change in the J value in Eq. (1) may accompany the structural change of Co–Mo–S. In their study on antiferromagnetic properties of di- μ -alkoxodicopper (II) complexes, Handa et al. [63] showed by ab initio MO calculations that the Cu–O–Cu angle affects the J value most effectively, but the other factors, such as dihedral angle, are much less effective. Their calculations qualitatively explain the magnetic property of numerous di- μ -alkoxodicopper (II) complexes cited in their paper. According to the experimental results cited in Ref. [63], the $-2J$ value is increased by about 170 K when the Cu–O–Cu angle is increased by 1°

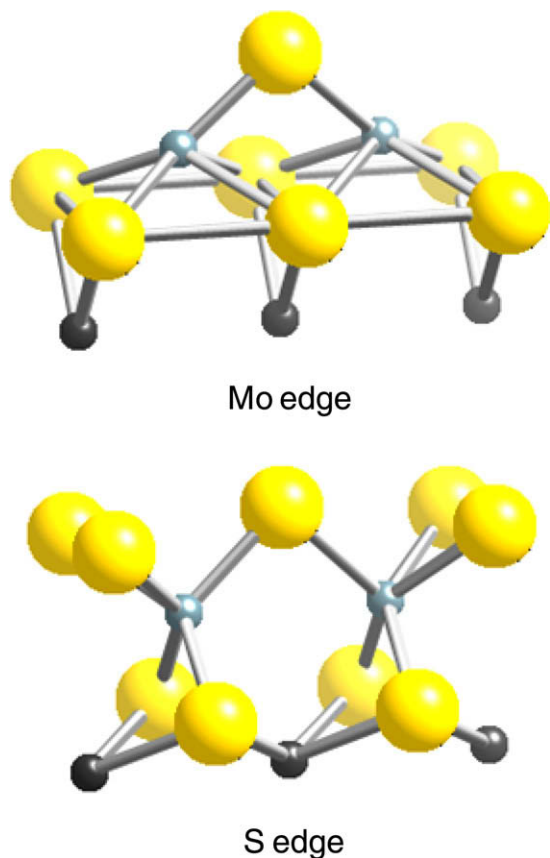


Fig. 11. Structure model of Co–Mo–S proposed from EXAFS and magnetic property. Large light ball (yellow), sulfur; small light ball (green), cobalt; and small dark ball (black), molybdenum. (For interpretation of the references in colour in this figure legend, the reader is referred to the web version of this article.)

between 99° and 104° . Accordingly, it is expected that the Co–S–Co angle and, as a consequence, Co–S, Co–Co and/or Co–Mo atomic distances in Co–Mo–S are slightly modified by the support and presulfidation temperature via MoS₂–O-support linkages, as is $-2J$. Scrutinizing the structural parameters given in Table 4, small but clear tendencies are actually recognized: a shorter Co–S atomic distance and a larger Co–Co atomic distance for the Co–Mo–S Type II catalysts, that is, Co/Mo/Si (873) and Co/Mo/Si (ATM) (673). The Co–S–Co angles estimated from the EXAFS parameters are 90.3° for Co/Mo/Al (673) and $91.4 \pm 0.1^\circ$ for Co/Mo/Si (873) and Co/Mo/Si (ATM) (673). The Co–S–Co angle is increased by about 1° by such a transformation of Co–Mo–S Type I to Type II. The increase in the Co–S–Co angle accounts for the increase in the $-2J$ value on the transformation, which is in agreement with the experimental results for the Cu (II) complexes and the theoretical calculations by Handa et al. [63]. A rather small change in the $-2J$ value by the change of Co–S–Co angle, that is, ca. $9 \text{ K}/1^\circ$, may be ascribed to the Co–S–Co angle of about 90° , where a much smaller effect is predicted compared to the angle of about 100° [63], and, in part, to the delocalization of electrons of Co (II) ($3d^7$) over the edge of MoS₂ particles. Since the Co–S atomic distance given in Table 4 is just an average value over the five Co–S bonds (cf. Fig. 11), the absolute value of Co–S–Co angle may be subjected to change, but we believe that the structure of Co–Mo–S is slightly modified by the MoS₂–O-support interactions, resulting in the difference in the intrinsic activity for HDS. The modifications in the electronic state and local structure of Co–Mo–S by the transformation of Type I to Type II are unambiguously evidenced by the systematic change in the XANES spectra shown in Fig. 8, which are not affected by possible artifacts in EXAFS analysis.

In agreement with the observations by Bouwens et al. [10], the intrinsic activity of Co–Mo–S increases as the CN of Co–S increases (Table 4). As discussed above, it is considered that the electronic modification of Co–Mo–S by MoS₂–O-support interactions also changes the adsorptive property for sulfur atoms or compounds. Finally, there is a clear tendency in Table 4 that the Debye–Waller-like factor (σ) is slightly smaller for Co–Mo–S Type II than for Type I, suggesting that the local structure of Co–Mo–S Type I is in a more disordered state than that of Type II due to MoS₂–O-support interactions. With Co–W–S, no notable change in the structural parameters is observed between Co/W/Si (673) and Co/W/Al (673), except for slightly larger σ values for the latter. This is consistent with similar TOF values for both catalysts (9.1 and 7.1 h^{-1} for the SiO₂-supported catalyst and Al₂O₃-supported catalyst, respectively).

4.5. Location of Co–Mo–S

It is very important to determine on which edge of MoS₂ the Co atoms are located as Co–Mo–S. On the basis of their STM study, Lauritsen et al. [46,64] and Topsøe [48], demonstrated that Co atoms are preferentially located on the $(\bar{1}010)$ S-edge of MoS₂ particles supported on Au(111) surface. DFT calculations [57,65] supported their results. Very recently, Krebs et al. [58] suggested through DFT calculations that Co atoms are located on both S- and Mo-edges of MoS₂ particles. In the present EXAFS analysis, unfortunately, we cannot determine the location of Co–Mo–S from the structural parameters (Fig. 11).

In the present study, we used the CVD technique to prepare Co/Mo/Si, in which the Co atoms are selectively and fully located on the edge of MoS₂ particles to form Co–Mo–S [22,40]. The amount of adsorption of Co(CO)₃NO on SiO₂ surface was negligibly small [22]. When we assume an appropriate geometrical model of MoS₂ particles, we can calculate the number of Mo atoms and hence that of Co atoms on the edge as a function of the particle size. We used a geometrical model of MoS₂ proposed by Kasztelan et al. [66] as such a model. The average size of MoS₂ particles given in Table 2 was used for the estimation of the ratio, $\text{Mo}_{\text{edge}}/\text{Mo}_{\text{total}}$ or (the total number of Mo atoms on the Mo- and S-edges)/(the total number of Mo atoms in the MoS₂ particle), assuming a regular hexagon morphology. When we assume that the number of Co atoms on the edge equals the number of the Mo atoms at a full coverage of Co–Mo–S, the Co/Mo atomic ratio can be calculated on the basis of the model. With the Co/Mo/Si catalysts presulfided at 673 and 973 K, the $\text{Mo}_{\text{edge}}/\text{Mo}_{\text{total}}$ ratios or Co/Mo ratios were calculated to be 0.28 and 0.27, respectively, which are in excellent agreement with the observed ratios 0.27 and 0.23 shown in Fig. 1. With W/Si (673) having 7.9 and 15.9 wt% W, we had reported the average sizes of 2.9 nm and 6.7 nm, respectively, for WS₂ particles by TEM [30]. The Co/W ratios were calculated to be 0.29 and 0.16 against the observed ratios 0.26 and 0.11, respectively [30]. Taking into consideration the simple model employed here and the accuracy of the average size of MoS₂ or WS₂ particles by TEM, these excellent agreements may be somewhat fortuitous, but it is very likely that the Co atoms occupy substitutional positions for Mo atoms on both Mo- and S-edges of MoS₂ (WS₂) particles rather than those on one of these edges. The present results are compatible with the DFT calculations by Krebs et al. [58], showing that a Co coverage on the S-edge is 100%, while that on the Mo-edge is 50% under HDS conditions. Different locations of Co in Co–MoS₂/Au(111) and Co/Mo(W)/Si may be ascribed to the different preparation methods and supports employed in the STM study by Lauritsen et al. [46,64] and in the present CVD study. It would be of great importance to determine the respective reactivity of the Co–Mo(W)–S structures on the Mo- and S-edges for HDS as well as their thermal stability during the reaction.

5. Conclusions

We studied SiO₂-supported Co–Mo and Co–W sulfide catalysts prepared by the CVD technique using Co(CO)₃NO as a precursor to Co sulfide to reveal the effect of the presulfidation temperature on the intrinsic activity, electronic states, and local structure of Co–Mo–S and Co–W–S. The Co/Mo(W) catalysts were characterized by TPS, XAFS, TEM, and magnetic measurements. The salient findings in the present study are as follows:

- Type II forms of Co–Mo–S and Co–W–S are prepared when Mo and W oxides are completely sulfided to MoS₂ and WS₂ particles.
- Co–W–S Type II is 1.6 times as active as Co–Mo–S Type II for the HDS of thiophene.
- The structure of Co–Mo–S is described as dinuclear Co sulfide clusters on the edge of MoS₂ particles regardless of the coverage of Co. It is likely that Co atoms are situated on both Mo- and S-edges of MoS₂ particles. The structure and location of Co–W–S are similar to those of Co–Mo–S.
- The electronic state of Co–Mo–S, as evaluated by the magnetic interaction between the Co atoms, is correlated with the structure and intrinsic activity for the HDS. As the $-2J$ value increases, the intrinsic activity of Co–Mo–S increases.
- The MoS₂–O-support interaction determines the electronic states of MoS₂ particles, and thereby the electronic state, local structure, and intrinsic activity of Co–Mo–S on the edge.

Acknowledgments

This study was partially supported by Grand-in-Aid for Scientific Research (16360404) from the Ministry of Education, Culture, Sport, Science, and Technology, Japan. We are grateful to Mr. Takeshi Ebihara (Cosmo Oil Comp.) for the TEM observations. We also express our sincere appreciation to Prof. Handa (Shimane University) for useful discussion.

References

- C. Song, *Catal. Today* 86 (2003) 211.
- D. Whitehurst, T. Isoda, I. Mochida, *Adv. Catal.* 42 (1998) 345.
- S. Eijsbouts, *Appl. Catal. A* 158 (1997) 53.
- H. Topsøe, B.S. Clausen, F.E. Massoth, in: J.R. Anderson, M. Boudard (Eds.), *Catalysis Science and Technology*, vol. 11, Springer, Berlin, 1996, p. 1.
- H. Topsøe, B.S. Clausen, *Catal. Rev. – Sci. Eng.* 26 (1984) 395.
- H. Topsøe, B.S. Clausen, N. Topsøe, E. Pedersen, *Ind. Eng. Chem. Fundam.* 25 (1986) 25.
- R. Prins, V.H.J. de Beer, G.A. Somorjai, *Catal. Rev. – Sci. Eng.* 31 (1989) 1.
- R. Candia, O. Sørensen, J. Villadsen, N. Topsøe, B.S. Clausen, H. Topsøe, *Bull. Soc. Chim. Belg.* 93 (1984) 763.
- J.A.R. van Veen, H.A. Colijn, P.A.J.M. Hendriks, A.J. van Welsenes, *Fuel Process. Technol.* 35 (1993) 137.
- S.M.A. Bouwens, F.B.M. van Zon, M.P. van Dijk, A.M. van der Kraan, V.H.J. de Beer, J.A.R. van Veen, D.C. Koningsberger, *J. Catal.* 146 (1994) 374.
- J.A.R. van Veen, E. Gerkema, A.M. van der Kraan, P.A.J.M. Hendriks, H. Beens, *J. Catal.* 133 (1992) 112.
- Usman, T. Yamamoto, T. Kubota, Y. Okamoto, *Appl. Catal. A* 328 (2007) 219.
- Usman, T. Kubota, Y. Araki, K. Ishida, Y. Okamoto, *J. Catal.* 227 (2004) 523.
- Usman, T. Kubota, Y. Okamoto, *Bull. Chem. Soc. Jpn.* 79 (2006) 637.
- J.A.R. van Veen, P.A.J.M. Hendriks, R.R. Andea, E.J.G.M. Romers, A.E. Wilson, *J. Phys. Chem.* 94 (1990) 5282.
- E.J.M. Hensen, V.H.J. de Beer, J.A.R. van Veen, R.A. van Santen, *Catal. Lett.* 84 (2002) 59.
- B. Hinnemann, J.K. Nørskov, H. Topsøe, *J. Phys. Chem. B* 109 (2005) 2245.
- C. Arrouvel, M. Breyse, H. Toulhoat, P. Raybaud, *J. Catal.* 232 (2005) 161.
- D. Costa, C. Arrouvel, M. Breyse, H. Toulhoat, P. Raybaud, *J. Catal.* 246 (2007) 325.
- H. Topsøe, R. Candia, N. Topsøe, B.S. Clausen, *Bull. Soc. Chim. Belg.* 93 (1984) 783.
- J.A.R. van Veen, E. Gerkema, A.M. van der Kraan, A. Knoester, *J. Chem. Soc., Chem. Commun.* (1987) 1684.
- Y. Okamoto, K. Ochiai, M. Kawano, K. Kobayashi, T. Kubota, *Appl. Catal. A* 226 (2002) 115.
- M.J. Vissenberg, Y. van der Meer, E.J.M. Hensen, V.H.J. de Beer, A.M. van der Kraan, R.A. van Santen, J.A.R. van Veen, *J. Catal.* 198 (2001) 151.
- G. Kishan, L. Coulier, J.A.R. van Veen, J.W. Niemantsverdriet, *J. Catal.* 200 (2001) 194.
- L. Coulier, G. Kishan, J.A.R. van Veen, J.W. Niemantsverdriet, *J. Phys. Chem. B* 106 (2002) 5897.
- T. Kubota, N. Hosomi, K. Bando, T. Matsui, Y. Okamoto, *Phys. Chem. Chem. Phys.* 5 (2003) 4510.
- Y. Okamoto, A. Kato, Usman, K. Sato, I. Hiromitsu, T. Kubota, *J. Catal.* 233 (2005) 16.
- K. Inamura, T. Takyu, Y. Okamoto, K. Nagata, T. Imanaka, *J. Catal.* 133 (1992) 498.
- Y. Okamoto, M. Kawano, T. Kawabata, T. Kubota, I. Hiromitsu, *J. Phys. Chem. B* 109 (2005) 288.
- T. Kubota, K. Sato, A. Kato, Usman, T. Ebihara, T. Fujikawa, Y. Arai, K. Ishida, Y. Okamoto, *Appl. Catal. A* 290 (2005) 17.
- S. Eijsbouts, L.C.A. van der Oetelaar, R.R. Puijenbroek, *J. Catal.* 229 (2005) 352.
- H.R. Reinhoudt, A.D. van Lahgeveld, P.J. Kooyman, R.M. Stockmann, R. Prins, H.W. Zandbergen, J.A. Moulijn, *J. Catal.* 179 (1998) 443.
- P.J. Kooyman, E.J.M. Hensen, A.M. de Jong, J.W. Niemantsverdriet, J.A.R. van Veen, *Catal. Lett.* 74 (2001) 49.
- P. Scheffer, P. Arnoldy, J.A. Moulijn, *J. Catal.* 112 (1998) 516.
- P. Arnoldy, J.A.M. van den Heijkant, G.D. de Bok, J.A. Moulijn, *J. Catal.* 92 (1985) 35.
- Usman, T. Kubota, I. Hiromitsu, Y. Okamoto, *J. Catal.* 247 (2007) 78.
- O. Kahn, *Molecular Magnetism*, VCH, Weinheim, 1993 (Chapter 6).
- J. Zhang, J.M. Soon, K.P. Loh, J. Yin, J. Ding, M.B. Sullivan, P. Wu, *Nano Lett.* 7 (2007) 2370.
- S.M.A.M. Bouwens, J.A.R. van Veen, D.C. Koningsberger, V.H.J. de Beer, R. Prins, *J. Phys. Chem.* 95 (1991) 123.
- Y. Okamoto, K. Ochiai, M. Kawano, T. Kubota, *J. Catal.* 222 (2004) 143.
- V. Rajamani, C.T. Prewitt, *Can. Mineral.* 13 (1975) 75.
- M.W.J. Craje, S.P.A. Louwers, V.H.J. de Beer, R. Prins, A.M. van der Kraan, *J. Phys. Chem.* 96 (1992) 5445.
- Usman, T. Kubota, Y. Okamoto, *Ind. Eng. Chem. Res.* 45 (2006) 3537.
- M. de Boer, A.J. Van Dillen, D.C. Koningsberger, J.W. Geus, M.A. Vuurman, I.E. Wacks, *Catal. Lett.* 11 (1991) 227.
- Y. Iwasawa, in: Y. Iwasawa (Ed.), *Tailored Metal Catalysts*, Reidel, Dordrecht, 1986, p. 1.
- J.V. Lauritsen, S. Helveg, E. Lægsgaard, I. Stengaard, B.S. Clausen, H. Topsøe, F. Besenbacher, *J. Catal.* 197 (2001) 1.
- J.V. Lauritsen, M. Nyberg, J.K. Nørskov, B.S. Clausen, H. Topsøe, E. Lægsgaard, F. Besenbacher, *J. Catal.* 224 (2004) 94.
- H. Topsøe, *Appl. Catal. A* 322 (2007) 3.
- M. Daage, R.R. Chianelli, *J. Catal.* 149 (1994) 415.
- P. Raybaud, *Appl. Catal. A* 322 (2007) 76, and references therein.
- J.-F. Paul, S. Cristol, E. Payen, *Catal. Today* 130 (2008) 139, and references therein.
- R.R. Chianelli, T.A. Pecoraro, T.R. Halbert, W.-H. Pan, E.I. Stiefel, *J. Catal.* 86 (1984) 226.
- R.R. Chianelli, *Catal. Rev. – Sci. Eng.* 26 (1984) 361.
- H. Toulhoat, P. Raybaud, *J. Catal.* 216 (2003) 63.
- C. Thomazeau, C. Geantet, M. Lacroix, M. Danot, V. Harle, P. Raybaud, *Appl. Catal. A* 322 (2007) 92.
- A.D. Gandubert, E. Krebs, C. Legens, D. Costa, G. Guillaume, P. Raybaud, *Catal. Today* 130 (2008) 149.
- H. Schweiger, P. Raybaud, H. Toulhoat, *J. Catal.* 212 (2002) 33.
- E. Krebs, B. Silvi, P. Raybaud, *Catal. Today* 130 (2008) 160.
- P. Raybaud, J. Hafner, G. Kresse, S. Kasztelan, H. Toulhoat, *J. Catal.* 190 (2000) 128.
- F. Mauté, A. Vallet, J. Bachelier, J.C. Duchet, J.C. Lavalley, *J. Catal.* 162 (1996) 88.
- Y. Okamoto, M. Kawano, T. Kubota, *J. Chem. Soc., Chem. Commun.* (2003) 1086.
- S.P.A. Louwers, R. Prins, *J. Catal.* 133 (1992) 94.
- M. Handa, N. Koga, S. Kida, *Bull. Chem. Soc. Jpn.* 61 (1988) 3853.
- J.V. Lauritsen, J. Kibsgaard, G.H. Olesen, P.G. Moses, B. Hinnemann, S. Helveg, J.K. Nørskov, B.S. Clausen, H. Topsøe, E. Lægsgaard, F. Besenbacher, *J. Catal.* 249 (2007) 220.
- L.S. Byskov, J.K. Nørskov, B.S. Clausen, H. Topsøe, *J. Catal.* 187 (1999) 109.
- S. Kasztelan, H. Toulhoat, J. Grimblot, J.P. Bonnelle, *Appl. Catal.* 13 (1984) 127.